Kent Academic Repository

In depth analysis of the conversion mechanism of TiSnSb vs. Li by operando triple edge X-ray Absorption Spectroscopy: a chemometric approach

Marcus Fehse,*,†,‡,¶ Ali Darwiche,§ Moulay T. Sougrati,§,‖ Erik M. Kelder,‡,¶

Alan V. Chadwick,⊥,¶ Maria Alfredsson,⊥,¶ Laure Monconduit,§,‖,¶ and Lorenzo

Stievano*,§,‖,¶

†Dutch-Belgian (DUBBLE), ESRF-The European Synchrotron, CS 40220, 38043 Grenoble Cedex 9, France.

‡Faculty of Applied Sciences, Delft University of Technology, Delft, Netherlands.

¶Alistore European Research Institute, Université de Picardie Jules Verne, 33 rue Saint Leu, 80039 Amiens Cedex, France.

§Institut Charles Gerhardt AIME (CNRS UMR 5253), Université de Montpellier, CC 1502, Pl. E. Bataillon, 34095 Montpellier Cedex 5, France.

‖Reseau sur le Stockage Electrochimique de l'Energie (RS2E), CNRS FR3459, 33 Rue Saint Leu, 80039 Amiens Cedex, France.

⊥School of Physical Sciences, University of Kent, CT2 7NH, UK.

E-mail: marcus.fehse@gmail.com; lorenzo.stievano@umontpellier.fr

Abstract

The electrochemical cycling mechanism of the ternary intermetallic TiSnSb, a

promising conversion-type negative electrode material for lithium batteries, was thoroughly studied by *operando* X-ray Absorption Spectroscopy (XAS) at three different absorption edges, *i.e.*, Ti, Sn and Sb K-edge. Chemometric tools such as Principal component analysis and Multivariate Curve Resolution-Alternating Least Squares were applied on the extensive data set, to extract the maximum contained information in the whole set of operando data. The evolution of the near-edge (XANES) fingerprint and of the extended fine-structure (EXAFS) of the XAS spectra confirms the reversibility of the conversion mechanism, revealing that Ti forms metallic nanoparticles upon lithiation and binds back to both Sn and Sb upon the following delithiation. The formation of both Li_7Sn_2 and Li_3Sb upon lithiation was also clearly confirmed. The application of chemometric tools allowed the identification of a time shift between the reaction processes of Sn and Sb lithiation, indicating that the two metals do not react at the same time, in spite of a certain overlap between their respective reaction. Furthermore, XANES and EXAFS fingerprint show that the Ti-Sn-Sb species formed after one complete lithiation/delithiation cycle is distinct from the starting material TiSnSb.

Keywords

1   Introduction

Electrode materials reacting with lithium via a conversion reaction hold the promise of surpassing energy density of today's commercially dominating insertion type electrode materials.[1] However, fast capacity decay and short cycle life are still major drawbacks of these materials.[2] In spite of these difficulties several several promising conversion-type electrode materials have been presented and studied in the last years, based on either oxides[2] or

2

p-group semi-metals such as tin[3–5] or antimony.[6–8]

In this last group of materials, the most promising one is surely the ternary intermetallic TiSnSb, which was proposed first by *Sougrati et al.*.[9] Since its introduction several studies have been carried out in order to elucidate the reaction mechanism, and identify intermediate compounds, as well as its limitations. *Marino et al.* investigated the role of the internal structure via comparative study of ternary intermetallic TiSnSb and composite of Ti/Sn/Sb. The authors show that the intimacy at the nanometric scale of the ternary compound compared to the micro scale of the composite is crucial for the reversible cycling capacity of this material.[10] The role of transition metal element was also studied by substituting Ti with Nb and measuring XAS under *operando* conditions, showing that Nb does not contribute to the exchange of electrons.[11] *Wilhelm et al.* and *Zhang et al.* showed that via optimization of electrode formulation and adequate choice of electrolyte salts and additives a highly reversible capacity of $450\,mAhg^{-1}$ for several hundreds of cycles at high C-rate is attainable for the TiSnSb electrodes.[12,13] This underlines TiSnSb's potential as high energy density anode material and strengthens the interest in this promising electrode material. Recent studies also stressed possible problems for the application in real batteries related to the instability of this material in the lithiated state upon long-time relaxation.[14]

Based on the findings of the studies cited above, the current understanding of the conversion mechanism can be expressed by Eq. 1. Of the three elements contained in TiSnSb, Ti does not alloy to lithium, whereas Sn and Sb are expected to react simultaneously with it upon discharge to form Li_7Sn_2 and Li_3Sb, respectively. While the global reaction is reversible, the first reduction is different from the subsequent cycles as characteristic for conversion reactions, and hence the pristine state of material is never recovered.
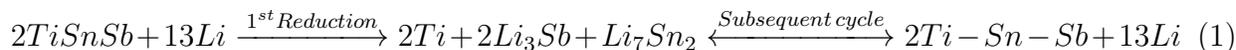
$$2TiSnSb+13Li \xrightarrow{1^{st}\,Reduction} 2Ti+2Li_3Sb+Li_7Sn_2 \xleftrightarrow{Subsequent\,cycle} 2Ti-Sn-Sb+13Li \quad (1)$$

3

Despite of the numerous studies on TiSnSb, the electrochemical conversion reaction on which the good cycling properties is based upon is still not fully understood. The role of the titanium, the stoichiometry, and order of occurrence of lithiated compounds, as well as the nature of the compound formed after the first complete cycle are still subject to debate.[9,11,14] The reactivity of Ti, in particular, has been a matter of debate: on the one hand, the big difference in reactivity of TiSnSb and SnSb vs. Li has suggested an active role of Ti, while on the other hand the study of its replacement with Nb has suggested that Ti is inactive and acts only as a mitigator or buffer for volume expansion.[9,11]

In order to clarify these open questions and provide a clearer view of this sluggish mechanism, it was decided to study the electrochemical reaction of TiSnSb with lithium by following the physicochemical state of the three elements at the same time by *operando* X-ray absorption spectroscopy (XAS). Since it is virtually impossible, however, to measure XAS spectra on the same sample in transmission at the three edges due to their very large difference in energy (4.996, 29.200 and 30.491 keV for Ti, Sn and Sb K-edge, respectively) two distinct experiments had to be arranged. In recently published studies, we have successfully applied chemometric tools such as principal component analysis (PCA) and Multivariate Curve Resolution - Alternating Least Squares (MCR-ALS)[15,16] to investigate complex and large spectral datasets in order to gain valuable insights on reaction mechanism and participating species;[17–21] these findings would have been reached only with difficulty by a conventional, manual data exploitation method. This alternative data analysis strategy was successfully used also to analyse the whole set of XAS spectra collected at the three edges. This approach, which allows in principle the unbiased extraction of all possible information from the *operando* data, enabled the stepwise reconstruction of the pure spectral components describing the evolution of the XAS spectra during the cycling of TiSnSb. In this way, a clear description of the electrochemically active species could be obtained, allowing a deeper understanding of the cycling mechanisms of this material.

4

2 Experimental

2.1 Material synthesis and electrode formulation

A detailed description of the preparation method of TiSnSb can be found elsewhere.[9] In short, TiSnSb is directly prepared by ball milling at high energy a mixture of Ti, Sn and Sb with the ratio of 1.1:1:1 for $24\,h$. The as synthesized material was thoroughly characterised by X-ray diffraction and ^{119}Sn Mössbauer spectroscopy, in agreement with the results of previous publications.[9,10,22]

Electrode films were prepared as described in detail in ref.[14] using TiSnSb, carboxymethyl cellulose (CMC) as the binder, and two conductive additives: vapor-grown carbon fibers (VGCF) and carbon black Y50A. The weight ratio of TiSnSb powder, CMC and additives was 70/12/9/9% (TiSnSb/CMC/Y50A/VGCF). In order to optimise the XAS signal-to-noise ratio and reduce self-absorption, a loading of $3\,mgcm^{-2}$ and self-supported configuration was chosen for the experiment at the Ti K-edge, whereas a sample with a loading of $20\,mgcm^{-2}$ on a copper current collector had to be prepared for the Sn/Sb K-edge measurement.

2.2 *Operando* X-ray absorption spectroscopy (XAS)

Operando measurements were carried out in transmission mode using a specifically designed *in situ* cell.[23] Due to the large difference in energy of the three absorption edges (4.996, 29.200 and $30.491\,keV$ for Ti, Sn and Sb K-edge, respectively), two distinct runs were organised. A cycling rate of C/5 was applied for the Ti XAS acquisition run and C/3.5 for the Sn-Sb one, where 1C corresponds to the reaction of $1\,mol$ Li with $1\,mol$ of TiSnSb in one hour. For the electrochemical cycling, a LiPF$_6$ $1\,M$ in EC:PC:3DMC electrolyte with 1% VC was used.

The acquisition time of single spectra was about $30\,min$. X-ray absorption spectra were acquired at *DUBBLE* Dutch-Belgian beamline 26A at *ESRF* (Grenoble, France). A Si(111) monochromator was used with an energy resolution of $1.7\,eV$ in combination with ion chamber detectors for the acquisition of XAS spectra at the three absorption edges.

2.3 Data analysis

After thorough alignment and cleaning of the XAS data sets, a statistical procedure based on PCA was applied in order to determine the minimum number of spectral components expressing the variance included in the whole set of data. The analysis was carried out separately for the spectra at the three edges. PCA is a chemometric factor analysis tool and is typically used to structure and simplify complex data sets by narrowing the multitude of variables with the least number of independent components. In our specific case this would be the number of spectral components necessary to express, by appropriate linear combinations, the whole set of spectra collected occurring during the electrochemical lithiation and delithiation of TiSnSb.

The number of principal components was subsequently fed to MCR-ALS, in order to reconstruct the "pure" XAS spectra and study their evolution upon electrochemical cycling. Several constrains where applied during the alternate fitting process: (i) non-negativity of the intensities of the components; (ii) unimodality for one of the components (in the case of Sb and Ti); (iii) closure (sum of all contributions always equal to 100 of the spectral intensity). More details about this procedure are available in other recently published works. [17,19–21]

3 Results and discussion

3.1 Evolution of the absorption edges during lithiation/delithiation

XAS spectra were acquired in the *operando* mode in two different experiments: in the first one Ti K-edge spectra were measured continuously (top), whereas in the second one the spectra of the *p*-group elements (bottom) were collected alternating the Sn and the Sb K-edge. The corresponding electrochemical curves are shown in Fig. 1(a), where the red and green circles indicate the collection of Sn and Sb spectra, respectively. For comparison, the typical galvanostatic electrochemical cycling curve of a TiSnSb optimised electrode measured

in a coin cell and its derivative are presented in Fig. 1(b) and inset, respectively.
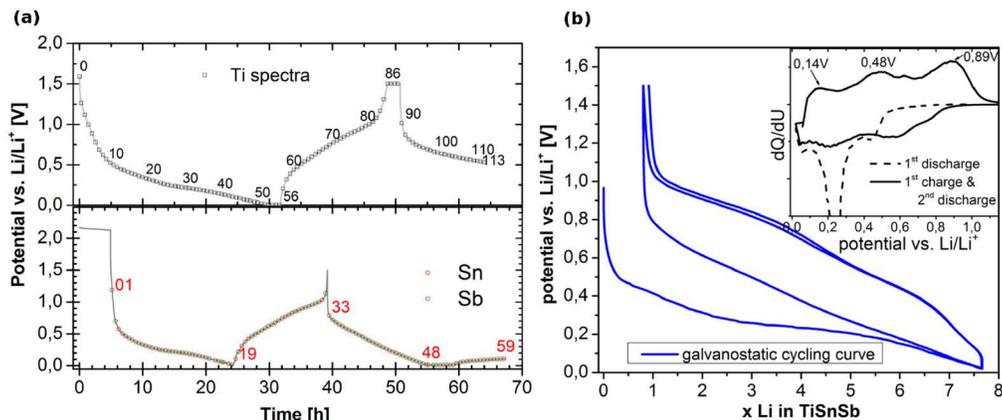

Figure 1: (a) Electrochemical signatures of subsequent lithiation, delithiation and (partial) lithiation at C/5 and C/3.5 for Ti (top) and Sn-Sb (bottom) XAS experiments, respectively. (b) Typical electrochemical cycling curve of TiSnSb and its derivative (inset).

The cycling curves reveal a fast voltage drop to about $0.5\,V$ where a sloping plateau starts governing the region of lithiation reaction. Upon charge a voltage jump is recorded before main delithiation takes place in the voltage range of 0.4-$1\,V$ with two slight plateaus at 0.5 and $0.9\,V$, which are clearly visible as peaks in the derivative (inset). Since the polarisation is somewhat larger in the Ti K-edge experiment, most probably due to the usage of a self-supported electrode, a floating process was performed at the end of each cycling stage in order to ensure that the electrode material reaches equilibrium.

The large hysteresis observed in these processes is an intrinsic characteristic feature of conversion mechanisms and is composed of a kinetic and thermodynamic contribution.[1,2,10] The derivative shows also very clearly that the first reduction reaction is distinct from the subsequent cycle which is linked to the transformation from micro sized to nanoscale material.[24] Furthermore the derivative of the galvanostatic oxidation curve reveals three peaks at ≈ 0.14, 0.48 and $0.89\,V$, respectively. The first peak can be attributed to the dissolution of the polymer/gel-like film whose formation is promoted by the highly reactive metallic nanograins formed during conversion.[8,25] The latter two peaks are attributed to the delithiation of the p-metal phases. The relatively large irreversible capacity during the first cycle

7

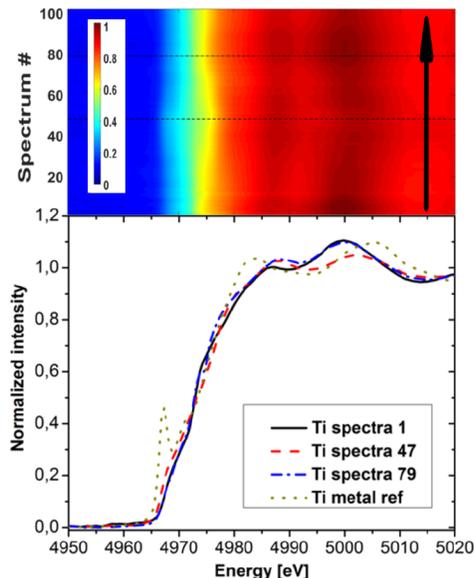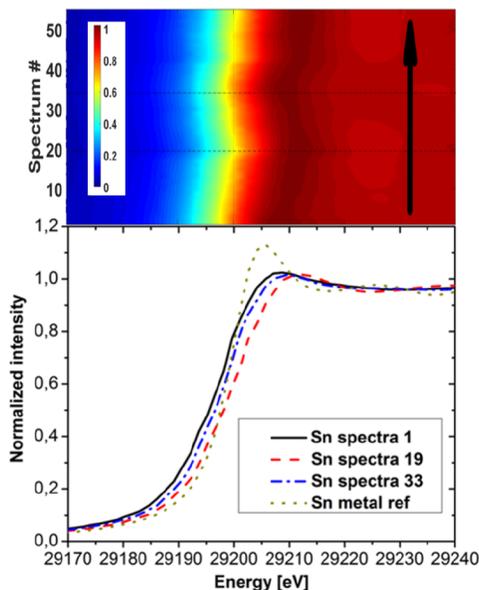is also quite typical of this type of mechanism.

Figure 2: Top: Evolution of Ti K-edge upon discharge and charge, the dashed line marks the end of 1st discharge (#47) while the dashed-dotted line marks the end of one complete cycle (#79). Bottom: Selection of XANES spectra acquired at key points of electrochemical cycling of Ti compared to Ti metal reference.

The evolution of the XANES upon consecutive first lithiation, delithiation and second lithiation are shown in Fig. 2, 3, 4 for Ti, Sn and Sb, respectively. The absorption edge of Ti is at the typical position of Ti in Ti metal and in Ti-based alloys, and changes only slightly upon electrochemical cycling. Such changes are much smaller than those observed for an effective change of oxidation state, e.g. $Ti^{+III/+IV}$ in titanium oxide.[26] This suggests that the chemical state of Ti does not vary substantially throughout the entire electrochemical process, and that Ti is mostly present in the metallic state. While it has already been previously assumed that Ti is inert in TiSnSb,[9,11] the here presented evolution of Ti XANES K edge under *operando* conditions is the first direct proof of its redox inactivity. The observed changes are largely reversible and can most likely be attributed to modifications of its local structural environment. In spite of the similar edge position, it is also noteworthy that at no point during electrochemical cycling the acquired Ti spectra resembles the spectrum of bulk Ti metal, even at the end of first lithiation (spectrum #47). This does not exclude,

8

however, the possible formation of Ti metal nanoparticles at the end of the lithiation, as usually observed in conversion reaction, since the absorption edge of metal nanoparticles is usually rather different from that of the corresponding bulk metal, with most oscillations and edge features strongly weakened and flattened out.[8]

The Sn and Sb XANES spectra reveal both a shift, as well as change in shape suggesting that they not only undergo a noticeable change in local structure but also in the electronic structure. The observed changes are largely reversible, as in the case of titanium. A comparison of the selected spectra with Sb metal and Sn metal reference shows that at no point during electrochemical cycling the electronic and local structure of the p-group metals are comparable to those of metallic bulk state. The K-edges of Sn and Sb are, however, very poor in information, showing only very broad features intrinsically related to the very short core-hole lifetime of their high energy absorption processes.

Figure 3: Top: Evolution of Sn K-edge upon discharge and charge, the dashed line marks the end of 1st discharge (#19) while the dashed-dotted line marks the end of one complete cycle (#33). Bottom: Selection of XANES spectra acquired at key points of electrochemical cycling of Sn compared to Sn metal reference.
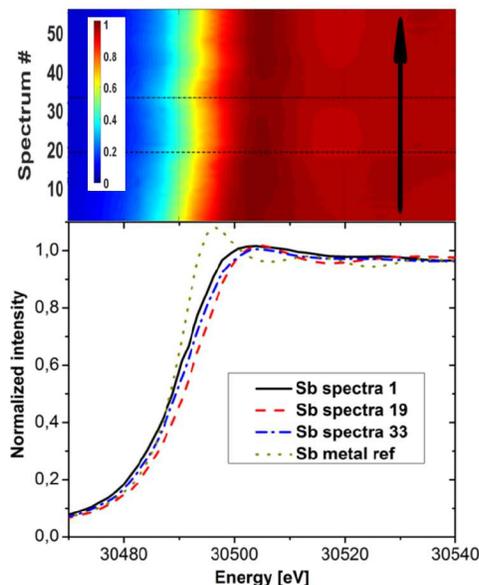
Figure 4: Top: Evolution of Sb K-edge upon discharge and charge, the dashed line marks the end of 1st discharge (#19) while the dashed-dotted line marks the end of one complete cycle (#33). Bottom: Selection of XANES spectra acquired at key points of electrochemical cycling of Sb compared to Sb metal reference.

3.2   Chemometric treatment of the EXAFS spectra

Since only limited information can be deducted from Ti and p-group metal XANES due to continuance in metallic state and short core-hole lifetimes, respectively, an in depth investigation of the entire data set is necessary. In Fig. 5 the variance plots from the PCA applied to the XAS data sets of the three different elements analysed separately are presented. In accordance with the mathematical definition of PCA, the first component is the dominating contributor to the total variance while the contribution of following components decreases gradually. The plots of Sn and Sb follow a similar slope revealing that over 99% of the total variance of the XAS can be described using only 3 principal components, for Ti the accumulated variance percentage of 3 components is just slightly below 99%. The residual is originating from experimental noise.

Although the PCA delivers not real XAS spectra but orthogonal mathematical functions, their number corresponds to the number of independent spectral components that can be used to describe the complete data set. In order to reconstruct the corresponding real
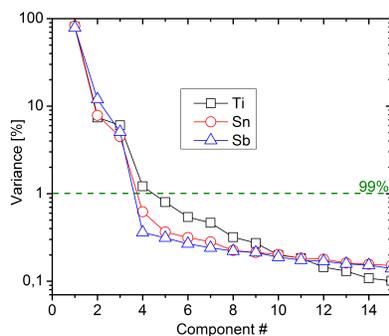
10

Figure 5: Variance plots obtained by the PCA analysis of the XAS spectra at the Ti (black), Sn (red), and Sb (blue) K-edge during the lithiation and delithiation of TiSnSb.

XAS components and their evolution, several methodologies are available. One of the most prominent is the multivariate curve resolution - alternated least squares (MCR-ALS) analysis tool.[27,28] *Tauler* was the first to apply this chemometric tool for the analysis of *in situ* spectroscopy data.[15]

Applying the MCR-ALS data analysis method on the XAS data sets of Ti, Sn and Sb led to the reconstruction of 3 components for each element which were subsequently treated as ordinary XAS data. The XANES and EXAFS regions are presented in Fig. 6 left and right, respectively. The evolution of their contribution to the total intensity upon lithiation and delithiation is shown in Fig. 7 for Ti (left) and Sn/Sb (right).

The three components obtained via MCR-ALS for Ti, shown in Fig. 6 (top left), are very similar to the spectra of pristine TiSnSb, of the end of charge (EOC) and of the end of discharge (EOD) states. They have similar XANES edge structures, in accordance with the meagre changes observed by inspecting the evolution of the XANES (*vide supra*, cf. Fig. 2). No significant shift of the edge position is observed underlining the fact that Ti remains in a chemical state close to the metallic one throughout the entire electrochemical process. The EOD component diverges from the other two after the main edge jump which indicates modifications of titanium's local structure. The pristine and EOC components largely overlap in energy-space (left) as well as in k-space (right) expressing high reversibility of the changes in the Ti structure. In spite of their similarities, the two latter components show substantial

11
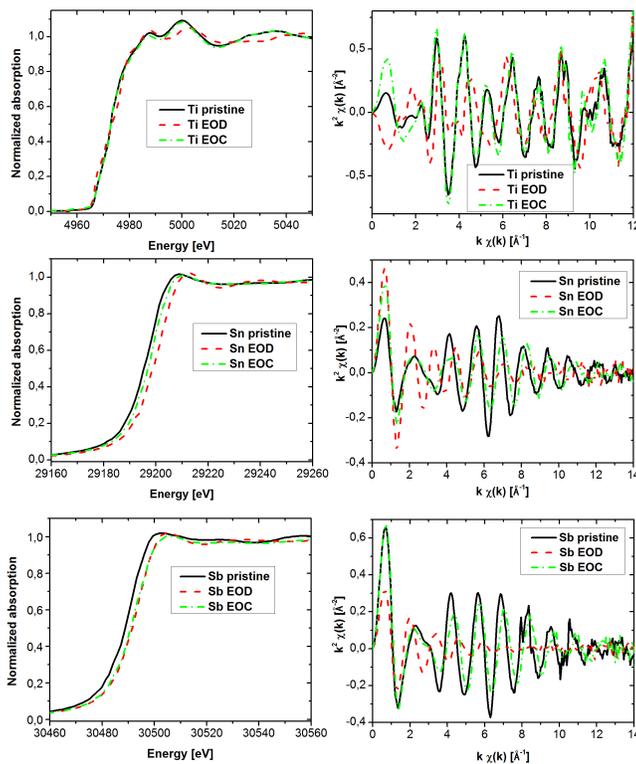
Figure 6: XANES (left) and EXAFS (right) regions of the Ti (top), Sn (middle), and Sb (bottom) K-edge spectral components obtained via the MCR-ALS analysis.

differences, indicating that a state similar but not identical to the pristine one is attained after a full discharge/charge cycle.

A similar behaviour is observed for both Sn and Sb spectra, where the three components also reach a maximum concentration in the pristine, EOD and EOC states. In the case of tin, shown in Fig. 6 (middle left), a shift in edge position to higher energy values upon lithiation can be observed (EOD), which is largely reversed upon delithiation (EOC). The difference between pristine and EOC component can be explained by incomplete lithium recovery (testified by the observed irreversible capacity) and/or formation of distinct Sn environments. The rapid fading of the EOD component in the k-space indicates the high

12

share of light scatterers (*e.g.*, lithium).

For the Sb components, shown in Fig. 6 (bottom), the observed trends are similar to Sn. However, the edge shape of EOD and EOC are more alike and widely overlap in energy space. In the *k*-space a rapid fading of the EOD component is observed which reflects its high share of light-scatterer contribution while pristine and EOC component follow similar oscillation indicating similarities in Sb states before and after one complete cycle.
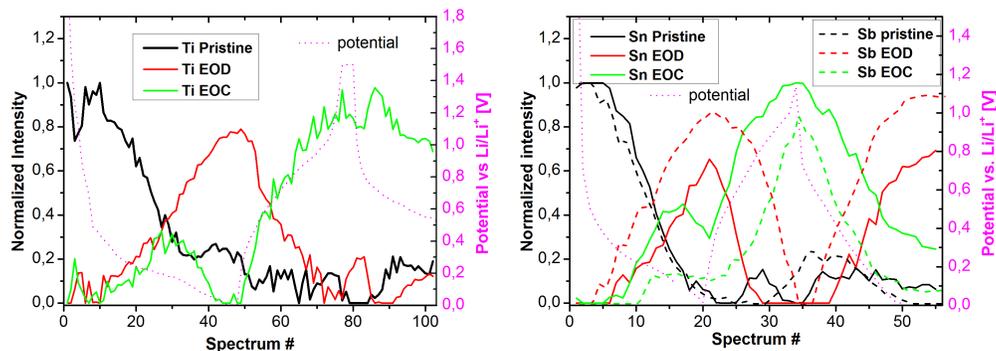

Figure 7: Evolution of the relative intensity of the of the MCR-ALS spectral components for Ti (left), Sn (right, full line) and Sb (right, dashed lines) of the K-edge spectra during the lithiation and delithiation of TiSnSb. The magenta dotted line indicates the potential curve corresponding to the acquisition of the spectra.

The concentration profiles of the three components obtained via MCR-ALS are shown in Fig. 7 for Ti (left) and Sn/Sb (right), respectively. For all three elements a similar main trend is observed. Before cycling a single component is present (pristine) which gradually decreases upon reduction while the EOD component increases and peaks when the lower voltage barrier is reached (Ti spectra 47, Sn-Sb spectra 20). Upon oxidation the EOD component gradually decreases and a new component EOC rises, reaching its maximum at upper voltage barrier (Ti spectra 80, Sn-Sb spectra 34). As stated above, the EOC component structurally resembles the pristine one however, it has distinct features of higher amorphisation degree and increased disorder. The growth of the EOD component at the cost of pristine component during first discharge reflects therefore the loss of long-range order upon lithiation. The fact that the pristine component does not rise to a significant share again after the completion of one whole cycle confirms that a new distinct form of Ti-Sn-Sb

13

is formed which is different than the starting material ternary intermetallic TiSnSb. The reduced smoothness of the titanium slopes compared to the Sn Sb ones is linked to the lower data quality of the Ti XAS spectra due to its low absorption edge energy.

When comparing the concentration profile of Sn and Sb with another, one notices that they only coincide partially. While the decrease of pristine component occurs simultaneously the growth of EOD and EOC follow a diverging pattern. Upon lithiation Sb starts earlier to form the EOD species and reaches a higher and broader maximum at the end of first reduction (spectra 20) than Sn. At this moment the Sn is composed of a mix of EOD and EOC component while for Sb EOD component is dominating. As the current is inversed and the lithiated species are oxidized one can observe that the onset of Sn EOC component formation is earlier and reaches a broader and higher maximum than Sb. The sharp peak of the Sb EOD component after one complete cycle (spectra 34) indicates that the electrochemical reaction had not yet reached equilibrium condition and floating of the cell at upper voltage barrier might have been necessary in order reach a more complete transformation. The second reduction of the p-group metals confirms the observation of the first one showing the increase of the EOD component with an earlier onset and broader and higher maximum for Sb compared to Sn.

These observed differences in the evolution of components demonstrate that the electrochemical lithiation and de-lithiation of Sn and Sb do not occur exactly simultaneously, but that the two processes are slightly shifted in potential. The potential offset corresponds well to the position of the two peaks observed in the derivative of the electrochemical cycling curve as can be seen in Fig. 8. This underlines the previous assumption that the peaks at ≈ 0.5 and $0.9\,V$ can be linked to the delithiation of Sn and Sb, respectively. The slight shift to higher potentials of the EOC derivative curves compared to the derivative of the electrochemical cell is linked to higher loading of the Sn-Sb *operando* electrode resulting in increased overpotential. The origin of the feature peaking at $\approx 0.15\,V$ has been assigned to the dissolution of polymer/gel like film, *vide supra*.
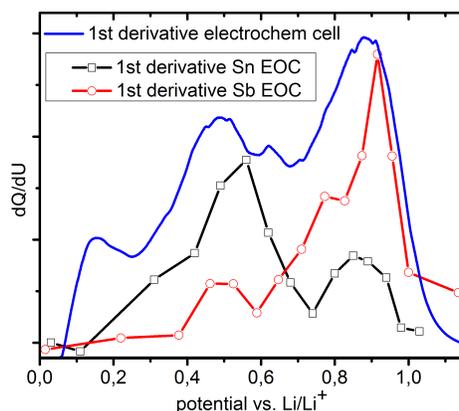
14

Figure 8: Derivatives of Sn and Sb EOC component formation from MCR-ALS and derivative of typical electrochemical cycling curve during charge.

To better understand the nature of the chemical species that correspond to the pristine, end of discharge (EOD) and end of charge (EOC) components, a detailed analysis of the EXAFS portion was carried out. The FT of the EXAFS regions of the components obtained via MCR-ALS are presented in Fig. 9. The results of the EXAFS fit for Ti, Sn, and Sb are presented in Tab. 1, 2, and 3, respectively. For the plots of the fits in FT and k-space please refer to S.I..

The most salient feature when comparing the FT of the components of the three elements in Fig. 9 is the reduced intensity of the EOD components in particular for the p-group metals. The low intensity for the p-group metal EOD component is due to the low scattering cross section of the lithiated species which dominate at this state. Subsequent delithiation leads to a rise in intensity due to the re-bonding with heavier scatterers. Although the intensity of the EOC intensity remains below the pristine value, the shape of the EOC and pristine component resemble one another, which illustrates similar local structural environment. In the case of the titanium the resemblance is particularly strong.

For the EXAFS fitting of Sn and Sb the pristine component only scattering contribution from TiSnSb were used, for Ti an additional 10% contribution of TiO_2 was included which remains unchanged throughout electrochemical reaction. The presence of slight amounts of
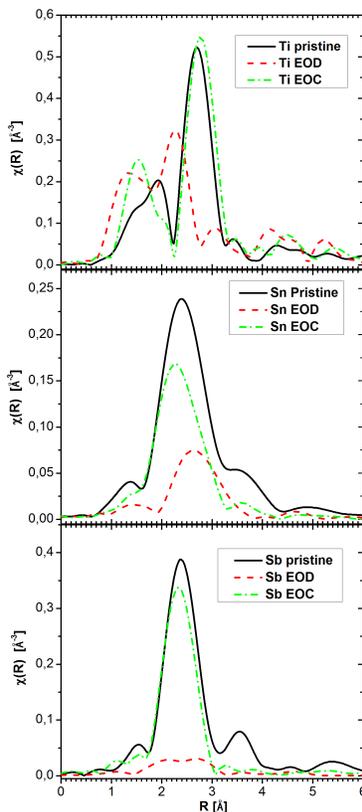
15

Figure 9: Fourier transforms (calculated with a k^3 weight) of the EXAFS region of the Ti (top), Sn (middle), and Sb (bottom) K-edge spectral components obtained by MCR-ALS analysis.

TiO_2 is justified by the starting stoichiometry used for the synthesis, which is performed using a slight excess of Ti. Lowest R-values (goodness of fit) values were achieved for the pristine component indicating the good accordance of the structural model with experimental data.

For the EOD Ti component, Ti nearest neighbours with a bond distance similar to Ti metal but with a lower coordination number dominate the scattering contribution, in line with the formation of Ti nanoparticles. Whereas minor contributions of Sn(Sb) and oxygen neighbours indicate the presence of small but detectable amounts of TiSnSb and TiO_2. The fitting of Sn EOD component was achieved with solely Li_7Sn_2 scattering contributions indicating the complete transformation of TiSnSb. An elevated *Debye-Waller* factor σ^2 is found for the first lithium shell, in line with the presence of very disordered lithiated

Table 1: EXAFS fitting parameters of MCR-ALS components of Ti K-edge

Component	Shell	N	R_{theo}[Å]	R_{fit} [Å]	σ^2 [Å]²	S
pristine	M-M	2	2.818[29]	2.72(3)	0.014(5)	0.38
	M-Sn/Sb	8	2.913[29]	2.78(1)	0.010(1)	
	M-O	6	1.959[30]	2.21(7)	0.006*	0.04*
EOD	M-M	2	2.818[29]	2.73(4)	0.024(4)	0.09(3)
	M-Sn/Sb	8	2.913[29]	2.85(4)	0.006*	
	M-O	6	1.959[30]	2.21(7)	0.006*	0.04*
	M-M$_{NP}$[1]	12	2.95[31]	2.81(4)	0.024(4)	0.29(3)
EOC	M-M	2	2.818[29]	2.74(5)	0.02(2)	0.35(9)
	M-Sn/Sb	8	2.913[29]	2.85(2)	0.008(4)	
	M-O	6	1.959[30]	2.1(2)	0.006*	0.04*
	M-M$_{NP}$[1]	12	2.95[31]	2.81(5)	0.02(2)	0.03

[1] Ti metal nanoparticles
* values without error have been fixed during the fit

species, with interatomic distances corresponding well to the values usually observed in Li_7Sn_2 and more generally in lithium tin compounds.[32] In the case of Sb EOD component, the main contribution was fitted with cubic β-Li_3Sb. However, a small contribution from Sn(Sb) neighbours (representing TiSnSb) had to be also included for a residual Me-Me contribution. No contribution from p-group metal-Ti bonds, reflecting the disconnection of p-group metal from Ti, was needed. The precision of XAS in the determination of number of next neighbors is relatively limited, therefore the presence of non-stoichiometric $Li_{2-x}Sb$ and Li_7Sn_2, as suggested by Li-NMR studies by *Johnston et al.* can neither be clearly proven nor ruled out based on our findings.[14]

For the EOC component of the p-group metals only TiSnSb contribution was used, which confirms their re-bonding with Ti upon delithiation. This re-bonding is also confirmed by Ti EOC component comprising a dominant TiSnSb and minor TiO_2 contribution. Whether the material that is formed after one complete electrochemical cycle is a mix of binary Ti p-group metal compounds or a ternary Ti-Sn-Sb-like compound can not be said with certainty since Sn and Sb are indistinguishable by XAS. However, the simultaneous re-bonding of p-group metals with Ti strongly point towards the latter.

Table 2: EXAFS fitting parameters of MCR-ALS components of Sn K-edge

Component	Shell	N	R_{theo}[Å]	R_{fit} [Å]	σ^2 [Å]^2	S
pristine	M-Ti	4	2.913[29]	2.913(4)	0.0136(7)	0.8[*]
	M-Sn/Sb$_1$	5	3.088[29]	3.14(1)	0.024(2)	
	M-Sn/Sb$_2$	5	3.362[29]	3.52(1)	0.024(2)	
EOD	M-Li$_1$	6	2.87[32]	2.81(4)	0.05(1)	0.8[*]
	M-Li$_2$	6	3.20[32]	3.32(1)	0.010(2)	
	M-Sn	0.5	2.99[32]	3.06(3)	0.010(4)	
EOC	M-Ti	4	2.913[29]	2.84(2)	0.0183(9)	0.8[*]
	M-Sn/Sb$_1$	6	3.088[29]	3.00(2)	0.024(2)	
	M-Sn/Sb$_2$	3	3.362[29]	3.31(4)	0.024(2)	

[*] values without error have been fixed during the fit

Table 3: EXAFS fitting parameters of MCR-ALS components of Sb K-edge

Component	Shell	N	R_{theo}[Å]	R_{fit} [Å]	σ^2 [Å]^2	S
pristine	M-Ti	4	2.913[29]	2.89(1)	0.0094(5)	0.8[*]
	M-Sn/Sb$_1$	2	3.088[29]	2.94(2)	0.029(3)	
	M-Sn/Sb$_2$	7	3.362[29]	3.62(2)	0.029(3)	
EOD	M-Li$_1$	6	2.84[33]	2.95(2)	0.020(2)	0.70(9)
	M-Li$_2$	6	3.28[33]	3.58(4)	0.020(2)	
	M-Sn/Sb^1	6	3.225[29]	3.46(4)	0.02(1)	0.10(9)
EOC	M-Ti	4	2.913[29]	2.82(1)	0.0121(6)	0.8[*]
	M-Sn/Sb$_1$	5	3.088[29]	2.96(2)	0.029(3)	
	M-Sn/Sb$_2$	5	3.362[29]	3.36(3)	0.029(2)	

[1] from TiSnSb not β-Li$_3$Sb
[*] values without error have been fixed during the fit

Generally fits at EOD reveal the lowest goodness of fit and highest error values of σ^2 indicating strong light-scatterer contribution and loss of long-range order upon lithiation. For the titanium EOD spectra best fit was obtained with a majority contribution of Ti nanoparticles, while TiO_2 content remains constant and minor TiSnSb contribution.

While the EXAFS spectra of pristine Sn and Sb reveal some contribution from second and third neighbor shell beyond 3.5 Å this is largely reduced in the corresponding EOD and EOC components which underlines the transformation to nanoconfined material upon first discharge.

4 Conclusion

Triple edge XAS were acquired under *operando* conditions and exploited using a chemometric approach including PCA and MCR-ALS. Our findings confirm that TiSnSb reacts with lithium through an authentic conversion reaction in which the *p*-group metals are electrochemical active while transition metal Ti reacts by reversibly forming Ti metal nanoparticles and binding back to the *p*-group metals. We present thus proof for the first time that Ti is inactive from the redox point of view, but undergoes a reversible structural changes from TiSnSb to Ti nanoparticles. EXAFS fitting results suggest the formation of Li_7Sn_2 and Li_3Sb upon lithiation accompanied by a complete amorphisation of the structure. This amorphisation starts on the pristine material already during the first lithiation. In spite of this general amorphisation, the whole electrochemical process is largely reversed during delithiation. Our findings strongly indicate the formation of ternary "Ti-Sn-Sb-like" compound after one complete electrochemical cycle with distinct structural properties from pristine state TiSnSb. The use of PCA and MCR-ALS enabled us to visualize that the lithiation and delithiation reaction of the *p*-group metals do not occur simultaneously but are slightly shifted, with the lithiation/delithiation reaction of Sb being centered at a slightly higher potentials than that of Sn. We attribute the presence of two plateaus in the electrochemical cycling to this potential shift in the reaction of the two *p*-group metals.

Acknowledgments

19

Supporting Information Available

EXAFS fits in FT and k-space of the three MCR-ALS components for each absorption edge, Ti, Sn, Sb are shown This material is available free of charge via the Internet at http://pubs.acs.org/.

References

(1) Cabana, J.; Monconduit, L.; Larcher, D.; Palacín, M. R. Beyond intercalation-based Li-ion batteries: the state of the art and challenges of electrode materials reacting through conversion reactions. *Adv. Mater.* **2010**, *22*, E170–92.

(2) Kraytsberg, A.; Ein-Eli, Y. A critical review-promises and barriers of conversion electrodes for Li-ion batteries. *J. Solid State Electrochem.* **2017**, 1–17.

(3) Sivasankaran, V.; Marino, C.; Chamas, M.; Soudan, P.; Guyomard, D.; Jumas, J.-C.; Lippens, P.-E.; Monconduit, L.; Lestriez, B. Improvement of intermetallics electrochemical behavior by playing with the composite electrode formulation. *J. Mater. Chem.* **2011**, *21*, 5076–5082.

(4) Vogt, L. O.; Villevieille, C. FeSn2 and CoSn2 Electrode Materials for Na-Ion Batteries. *J. Electrochem. Soc.* **2016**, *163*, A1306–A1310.

(5) Vogt, L. O.; Villevieille, C. Elucidation of the reaction mechanisms of isostructural FeSn2 and CoSn2 negative electrodes for Na-ion batteries. *J. Mater. Chem. A* **2017**, *5*, 3865–3874.

(6) Villevieille, C.; Ionica-Bousquet, C.-M. M.; Ducourant, B.; Jumas, J.-C.; Monconduit, L. NiSb2 as negative electrode for Li-ion batteries: An original conversion reaction. *J. Power Sources* **2007**, *172*, 388–394.

(7) Villevieille, C.; Ionica-Bousquet, C. M.; De Benedetti, A.; Morato, F.; Pierson, J.-F.; Simon, P.; Monconduit, L. Self supported nickel antimonides based electrodes for Li ion battery. *Solid State Ionics* **2011**, *192*, 298–303.

(8) Marino, C.; Fraisse, B.; Womes, M.; Villevieille, C.; Monconduit, L.; Stievano, L. At the Heart of a Conversion Reaction: An Operando X-ray Absorption Spectroscopy

Investigation of NiSb2 , a Negative Electrode Material for Li-Ion Batteries. *J. Phys. Chem. C* **2014**, *118*, 27772–27780.

(9) Sougrati, M. T.; Fullenwarth, J.; Debenedetti, A.; Fraisse, B.; Jumas, J. C.; Monconduit, L. TiSnSb a new efficient negative electrode for Li-ion batteries: mechanism investigations by operando-XRD and Mössbauer techniques. *J. Mater. Chem.* **2011**, *21*, 10069.

(10) Marino, C.; Sougrati, M. T.; Gerke, B.; Pöttgen, R.; Huo, H.; Ménétrier, M.; Grey, C. P.; Monconduit, L. Role of structure and interfaces in the performance of TiSnSb as an electrode for Li-ion batteries. *Chem. Mater.* **2012**, *24*, 4735–4743.

(11) Marino, C.; Sougrati, M. T.; Darwiche, A.; Fullenwarth, J.; Fraisse, B.; Jumas, J. C.; Monconduit, L. Study of the series Ti1-yNbySnSb with 0 y 1 as anode material for Li-ion batteries. *J. Power Sources* **2013**, *244*, 736–741.

(12) Wilhelm, H.; Marino, C.; Darwiche, A.; Monconduit, L.; Lestriez, B. Significant electrochemical performance improvement of TiSnSb as anode material for Li-ion batteries with composite electrode formulation and the use of VC and FEC electrolyte additives. *Electrochem. commun.* **2012**, *24*, 89–92.

(13) Zhang, W.; Ghamouss, F.; Mery, A.; Lemordant, D.; Dedryvère, R.; Monconduit, L.; Martinez, H. Improvement of the stability of TiSnSb anode under lithiation using SEI forming additives and room temperature ionic liquid/DMC mixed electrolyte. *Electrochim. Acta* **2015**, *170*, 72–84.

(14) Johnston, K. E.; Sougrati, M. T.; Stievano, L.; Darwiche, A.; Dupré, N.; Grey, C. P.; Monconduit, L. Effects of Relaxation on Conversion Negative Electrode Materials for Li-Ion Batteries: A Study of TiSnSb Using 119 Sn Mössbauer and 7 Li MAS NMR Spectroscopies. *Chem. Mater.* **2016**, *28*, 4032–4041.

(15) Tauler, R. Multivariate curve resolution applied to second order data. *Chemom. Intell. Lab. Syst.* **1995**, *30*, 133–146.

(16) Voronov, A.; Urakawa, A.; van Beek, W.; Tsakoumis, N. E.; Emerich, H.; Rønning, M. Multivariate curve resolution applied to in situ X-ray absorption spectroscopy data: An efficient tool for data processing and analysis. *Anal. Chim. Acta* **2014**, *840*, 20–27.

(17) Iadecola, A.; Perea, A.; Aldon, L.; Aquilanti, G.; Stievano, L. Li deinsertion mechanism and Jahn-Teller distortion in LiFe0.75Mn0.25PO4: an operando X-ray absorption spectroscopy investigation. *J. Phys. D Appl. Phys.* **2017**, *50*, 144004.

(18) Giorgetti, M.; Mignani, A.; Aquilanti, G.; Conti, P.; Fehse, M.; Stievano, L. Structural and electronic studies of metal hexacyanoferrates based cathodes for Li rechargeable batteries. *J. Phys. Conf. Ser.* **2016**, *712*, 012127.

(19) Loaiza, L. C.; Salager, E.; Louvain, N.; Boulaoued, A.; Iadecola, A.; Johansson, P.; Stievano, L.; Seznec, V.; Monconduit, L. Understanding the lithiation/delithiation mechanism of Si(1x)Ge(x) alloys. *J. Mater. Chem. A* **2017**, *5*, 12462–12473.

(20) Landa-Medrano, I.; Sorrentino, A.; Stievano, L.; de Larramendi, I. R.; Pereiro, E.; Lezama, L.; Rojo, T.; Tonti, D. Architecture of Na-O2 Battery Deposits Revealed by Transmission X-ray Microscopy. *Nano Energy* **2017**, *37*, 224–231.

(21) Broux, T.; Bamine, T.; Simonelli, L.; Stievano, L.; Fauth, F.; Ménétrier, M.; Carlier, D.; Masquelier, C.; Croguennec, L. VIV Disproportionation Upon Sodium Extraction from Na3V2(PO4)2F3 Observed by Operando X-ray Absorption Spectroscopy and Solid-State NMR. *J. Phys. Chem. C* **2017**, *121*, 4103–4111.

(22) Marino, C.; Darwiche, A.; Dupré, N.; Wilhelm, H. A.; Lestriez, B.; Martinez, H.; Dedryvère, R.; Zhang, W.; Ghamouss, F.; Lemordant, D.; Monconduit, L. Study of the Electrode/Electrolyte Interface on Cycling of a Conversion Type Electrode Material in Li Batteries. *J. Phys. Chem. C* **2013**, 130911150533004.

(23) Leriche, J. B.; Hamelet, S.; Shu, J.; Morcrette, M.; Masquelier, C.; Ouvrard, G.; Zerrouki, M.; Soudan, P.; Belin, S.; Elkaïm, E.; Baudelet, F. An electrochemical cell for operando study of lithium batteries using synchrotron radiation. *J. Electrochem. Soc.* **2010**, *157*, A606–A610.

(24) Khatib, R.; Dalverny, A. L.; Saubaneàre, M.; Gaberscek, M.; Doublet, M. L. Origin of the voltage hysteresis in the cop conversion material for Li-ion batteries. *J. Phys. Chem. C* **2013**, *117*, 837–849.

(25) Laruelle, S.; Grugeon, S.; Poizot, P.; Dolle, M.; Dupont, L.; Tarascon, J.-M. On the Origin of the Extra Electrochemical Capacity Displayed by MO/Li Cells at Low Potential. *J. Electrochem. Soc.* **2002**, *149*, A627.

(26) Fehse, M.; Monconduit, L.; Fischer, F.; Tessier, C.; Stievano, L. Study of the insertion mechanism of lithium into anatase by operando X-ray diffraction and absorption spectroscopy. *Solid State Ionics* **2014**, *268*, 252–255.

(27) Jaumot, J.; Gargallo, R.; De Juan, A.; Tauler, R. A graphical user-friendly interface for MCR-ALS: A new tool for multivariate curve resolution in MATLAB. *Chemom. Intell. Lab. Syst.* **2005**, *76*, 101–110.

(28) Jaumot, J.; de Juan, A.; Tauler, R. MCR-ALS GUI 2.0: New features and applications. *Chemom. Intell. Lab. Syst.* **2015**, *140*, 1–12.

(29) Dashjav, E.; Kleinke, H. Sn/Sb atom ordering in the ternary stannide-antimonide TiSnSb. *J. Solid State Chem.* **2003**, *176*, 329–337.

(30) Cromer, D. T.; Herrington, K. The Structures of Anatase and Rutile. *J. Am. Chem. Soc.* **1955**, *77*, 4708–4709.

(31) Wyckoff, R. W. G. *Crystal Structures*, 2nd ed.; Interscience Publishers: New York, 1963; pp 7–83.

(32) Robert, F.; Lippens, P.-E.; Olivier-Fourcade, J.; Jumas, J.-C.; Gillot, F.; Morcrette, M.; Tarascon, J.-M. Mössbauer spectra as a fingerprint in tinlithium compounds: Applications to Li-ion batteries. *J. Solid State Chem.* **2007**, *1180*, 339–348.

(33) Villevieille, C.; Fraisse, B.; Womes, M.; Jumas, J.-C.; Monconduit, L. A new ternary Li4FeSb2 structure formed upon discharge of the FeSb2/Li cell. *J. Power Sources* **2009**, *189*, 324–330.